Heat Transfer—Asian Research, **42** (2), 2013

Cross-Diffusion Effects on Mixed Convection from an Exponentially Stretching Surface in Non-Darcy Porous Medium

D. Srinivasacharya[1] and Ch. RamReddy[2]
[1]Department of Mathematics, National Institute of Technology, Warangal, A.P., India
[2]Department of Mathematics, National Institute of Technology, Rourkela, Odisha, India

The Soret and Dufour effects on mixed convection flow and heat and mass transfers from an exponentially stretching surface in a quiescent fluid-saturated non-Darcy porous medium is studied. Stretching velocity, wall temperature, and wall concentration are assumed to have specific exponential function forms. The governing partial differential equations are transformed into ordinary differential equations using similarity transformations and then solved numerically using an implicit finite difference scheme known as the Keller-box method. The present results are found to be in excellent agreement with previously published work on various special cases of the problem. The influence of buoyancy, Soret and Dufour numbers, and Darcy and non-Darcy parameters on the convective transport in the boundary layer region is analyzed. Also, the numerical values of the skin friction, heat, and mass transfer coefficients for different values of governing parameters are also tabulated. © 2013 Wiley Periodicals, Inc. Heat Trans Asian Res, 42(2): 111–124, 2013; Published online 8 January 2013 in Wiley Online Library (wileyonlinelibrary.com/journal/htj). DOI 10.1002/htj.21032

Key words: mixed convection, boundary layer flow, non-Darcy porous medium, exponentially stretching surface, Soret and Dufour effects

1. Introduction

The study of flow, heat, and mass transfer in the boundary layer of a continuously stretching surface with a given temperature and concentration distributions moving in an otherwise quiescent fluid medium has attracted the attention of researchers for the past few decades due to its numerous industrial and engineering applications. In particular, an extradite from a die is drawn and simultaneously stretched into a sheet, which is then solidified through quenching or gradual cooling by direct contact with water. Annealing and thinning of copper wires is another example. In all these cases, the quality of the final product depends on the rate of heat transfer at the stretching surface. Both the kinematics of stretching and the simultaneous heating or cooling during such processes has a decisive influence on the quality of the final products. After the pioneering works of Sakiadis [1], several researchers [2–5] discussed the problem of boundary layer flow of a stretching surface to obtain the thermal and kinematic behavior by considering the different forms of stretching velocity. There has been a renewed interest in convective heat and mass transfer in porous media due to diverse applications, such as thermal insulation, extraction of crude oil and chemical catalytic reactors, etc.

A detailed review of convective heat transfer in Darcian and non-Darcian porous medium can be found in the book by Nield and Bejan [6]. Several authors, Layek et al. [7] and Hayat et al. [8] to mention but few, have studied the convective heat and mass transfer over a different surface geometries in a fluid-saturated porous media.

In practical situations, the flow over a continuous material moving through a quiescent fluid is induced by the movement of the solid material and by thermal buoyancy. Therefore, these two mechanisms, surface motion and buoyancy force, will determine the momentum and thermal transport processes. The thermal buoyancy force arising due to the heating or cooling of a continuously moving surface, under some circumstances, may alter significantly the flow and thermal fields and thereby the heat transfer behavior in the manufacturing process. By considering the effect of buoyancy, Ali and Al-Yousef [9] analyzed mixed convection heat transfer from a uniformly stretching vertical surface with general power function form for stretching velocity of the wall and with surface suction/injection. Partha et al. [10] presented a similarity solution for mixed convection flow and heat transfer from an exponentially stretching surface by considering viscous dissipation effect in the medium. They showed that the buoyancy and viscous dissipation have significant influence on the non-dimensional skin friction and heat transfer coefficient. Recently, Pal [11] performed an analysis to describe mixed convection heat transfer in the boundary layers on an exponentially stretching continuous surface with an exponential temperature distribution in the presence of a magnetic field, viscous dissipation, and internal heat generation/absorption.

The Soret effect (thermal diffusion), the occurrence of a diffusion flux due to a temperature gradient, and the Dufour effect (diffusion-thermo), the occurrence of a heat flux due to a chemical potential gradient, become very significant when the temperature and concentration gradients are very large. Generally these effects are considered as second-order phenomenon and may become significant in areas such as hydrology, petrology, geosciences, etc. The importance of these effects in convective transport in clear fluids has been studied by Eckert and Drake [12], Dursunkaya and Worek [13], and Kafoussias and Williams [14]. El-Aziz [15] investigated the combined effects of thermal-diffusion and diffusion-thermo on MHD heat and mass transfer over a permeable stretching surface with thermal radiation. Ahmed [16] discussed free convective heat and mass transfer of an incompressible, electrically conducting fluid over a stretching sheet in the presence of suction and injection with thermal-diffusion and diffusion-thermo effects. A study has been carried out to analyze the combined effects of Soret and Dufour on unsteady MHD non-Darcy mixed convection over a stretching sheet embedded in a saturated porous medium in the presence of thermal radiation, viscous dissipation, and first-order chemical reaction by Pal and Mondal [17].

Thus, motivated by the above investigations and applications mentioned, the purpose of the present work is to investigate the Soret and Dufour effects on mixed convection heat and mass transfer from an exponentially stretching surface in a quiescent fluid-saturated non-Darcy porous medium. The free stream flow, wall temperature, and wall concentration are given specific forms of profiles which permit a similarity solution. The Keller-box method given in the works of Cebeci and Bradshaw [18] and Na [19] is employed to solve the non-linear system in the problem. The effects of the mixed convection parameter, Forchheimer number, Darcy number, Soret and Dufour numbers. and also X-location are examined and are displayed through graphs. Also, the effects of skin friction, the heat and mass transfer coefficient, are illustrated in tabular form for various parameters. The results are compared with relevant results in the existing literature and are found to be in good agreement.

Nomenclature

B: buoyancy ratio
b: Forchheimer constant (geometrical)
C: concentration
C_f: skin friction coefficient
C_0: concentration parameter of the stretching surface
C_p: concentration susceptibility
C_s: specific heat capacity (isobaric)
C_w: wall concentration
C_∞: ambient concentration
D: solutal diffusivity
Da: Darcy number
D_f: Dufour number
Fs: Forchheimer number
F: reduced stream function
g^*: gravitational acceleration
Gr: thermal Grashof number
k: thermal conductivity
K_p: permeability of porous medium
K_T: thermal diffusion ratio
L: characteristic length of the plate
Nu_x: local Nusselt number
Pr: Prandtl number
Re: Reynolds number
Re_x: local Reynolds number
Ri: mixed convection parameter
Sc: Schmidt number
Sh_x: local Sherwood number
S_r: Soret number
T: temperature
T_m: mean temperature
T_0: temperature parameter of the stretching surface
T_w: wall temperature
T_∞: ambient temperature
U_*: characteristic velocity
u_0: velocity parameter of the stretching surface
u_∞: free stream velocity
u, v: velocity components in x and y directions
X: X- location
x, y: coordinates along and normal to the plate

Greek Letters

α: thermal diffusivity
β_T, β_C: coefficients of thermal and solutal expansion

η: similarity variable
ε: porosity
θ: dimensionless temperature
ϕ: dimensionless concentration
μ: dynamic viscosity
ν: kinematic viscosity
ρ: density of the fluid
τ_w: wall shear stress
ψ: stream function

Subscripts

w: wall condition
∞: ambient condition
C: concentration
T: temperature

Superscript

$'$: differentiation with respect to η

2. Mathematical Formulation

Consider a steady, two-dimensional, laminar flow, and mixed convection heat and mass transfer from an impermeable plane vertical wall stretching with velocity $u_w(x)$, temperature distribution $T_w(x)$, and concentration distribution $C_w(x)$ embedded in a stable, quiescent incompressible fluid-saturated non-Darcy porous medium of constant temperature T_∞ and concentration C_∞ as shown in Fig. 1. The x-axis is directed along the continuous stretching surface and points in the direction of motion and the y-axis is perpendicular to it. Assume that the fluid and the porous medium have constant physical properties. The fluid flow is moderate and the permeability of the medium is low so that the Forchheimer flow model is applicable and the boundary effect is neglected. The fluid and

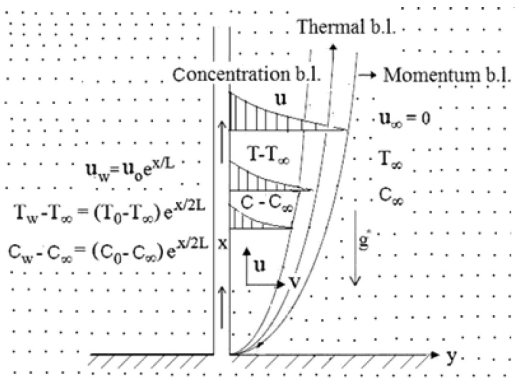

Fig. 1. Physical model and coordinate system.

the porous medium are in local thermodynamical equilibrium. In addition, the Soret and Dufour effects are considered.

Assuming that the Boussinesq and boundary layer approximations hold and using the Darcy–Forchheimer model and Dupuit–Forchheimer relationship [6], the governing equations for the viscous fluid-saturated non-Darcy porous medium in the presence of Soret and Dufour effects [14] are given by

$$\frac{\partial u}{\partial x}+\frac{\partial v}{\partial y}=0 \tag{1}$$

$$\frac{1}{\varepsilon^2}\left(u\frac{\partial u}{\partial x}+v\frac{\partial u}{\partial y}\right)=\frac{\nu}{\varepsilon}\frac{\partial^2 u}{\partial y^2}+g^*\left(\beta_T(T-T_\infty)+\beta_C(C-C_\infty)\right)-\frac{\nu}{K_P}u-\frac{b}{K_P}u^2 \tag{2}$$

$$u\frac{\partial T}{\partial x}+v\frac{\partial T}{\partial y}=\alpha\frac{\partial^2 T}{\partial y^2}+\frac{DK_T}{C_S C_P}\frac{\partial^2 C}{\partial y^2} \tag{3}$$

$$u\frac{\partial C}{\partial x}+v\frac{\partial C}{\partial y}=D\frac{\partial^2 C}{\partial y^2}+\frac{DK_T}{T_m}\frac{\partial^2 T}{\partial y^2} \tag{4}$$

where u and v are the velocity components in x and y directions, respectively, T is the temperature, C is the concentration, g^* is the acceleration due to gravity, ρ is the density, ν is the kinematic viscosity, μ is the dynamic coefficient of viscosity, b is the Forchheimer constant, K_P is the permeability, ε is the porosity, β_T is the coefficient of thermal expansion, β_C is the coefficient of solutal expansions, α is the thermal diffusivity, D is the solutal diffusivity of the medium, C_P is the specific heat capacity, C_S is the concentration susceptibility, T_m is the mean fluid temperature, and K_T is the thermal diffusion ratio. The last two terms on the right-hand side of Eq. (2) stand for the first-order (Darcy) resistance and second-order porous inertia resistance, respectively. The last term on the right-hand side of the energy equation (3) and diffusion equation (4) signifies the Dufour or diffusion-thermo effect and the Soret or thermal-diffusion effect, respectively.

The boundary conditions are

$$u=u_w(x), v=0, \mathrm{T}=\mathrm{T_w(x)}, \mathrm{C}=\mathrm{C_w(x)} \quad \text{at} \quad y=0 \tag{5a}$$

$$u=0, T=T_\infty, C=C_\infty \quad \text{as} \quad y\to\infty \tag{5b}$$

where the subscripts w and ∞ indicate the conditions at the wall and at the outer edge of the boundary layer, respectively.

The stretching velocity $u_w(x)$, exponential temperature distribution $T_w(x)$, and exponential concentration distribution $C_w(x)$ are defined as

$$u_w(x)=u_0 e^{x/L} \tag{6}$$

$$T_w(x)=T_\infty+(T_0-T_\infty)e^{x/2L} \tag{7}$$

$$C_w(x)=C_\infty+(C_0-C_\infty)e^{x/2L} \tag{8}$$

where u_0 is the velocity parameter of the stretching surface, and T_0 is the parameter of the temperature distribution whereas C_0 is the parameter of the concentration distribution in the stretching surface.

In view of the continuity equation (1), defining the stream function ψ such that

$$u = \frac{\partial \psi}{\partial y},\ v = -\frac{\partial \psi}{\partial x} \tag{9}$$

substituting Eq. (9) in Eqs. (2)–(4) and then using the following local similarity transformations

$$\left.\begin{aligned} &\eta = \frac{\mathrm{Re}}{2}\frac{y}{L}e^{x/2L},\ \psi = \sqrt{2}\,\nu\,\mathrm{Re}^{1/2}e^{x/2L}\,f(\eta) \\ &T(x,y) = T_\infty + (T_0 - T_\infty)e^{x/2L}\,\theta(\eta), C(x,y) = C_\infty + (C_0 - C_\infty)e^{x/2L}\,\phi(\eta) \end{aligned}\right\} \tag{10}$$

the governing equations become

$$\frac{1}{\varepsilon}f''' + \frac{1}{\varepsilon^2}\left(f\,f'' - 2f'^2\right) + 2\,Ri\;e^{-3X/2}(\theta + B\,\phi) - \frac{2}{Da.\mathrm{Re}}e^{-X}f' - \frac{2.Fs}{Da}f'^2 = 0 \tag{11}$$

$$\frac{1}{\mathrm{Pr}}\theta'' + f\,\theta' - f'\theta + D_f\phi'' = 0 \tag{12}$$

$$\frac{1}{Sc}\phi'' + f\,\phi' - f'\phi + S_r\theta'' = 0 \tag{13}$$

where the primes indicate partial differentiation with respect to η alone, L is the characteristic length of the plate, $X = x/L$ is the X-location, $Gr = g^*\beta_T(T_0 - T_\infty)L^3/\nu^2$ is the thermal Grashof number, $\mathrm{Re} = u_0L/\nu$ is the Reynolds number, $Da = K_P/L^2$ is the Darcy number, $Fs = b/L$ is the Forchheimer number, $Ri = Gr/\mathrm{Re}^2$ is the mixed convection parameter, which represents the ratio of buoyancy forces to the inertia forces and is used to delineate the free, forced, and mixed convection regimes. When $Ri = 0$, the flow becomes a forced convection flow and when Ri is large, the flow becomes a free convection flow. $B = \beta_C(C_0 - C_\infty)/\beta_T(T_0 - T_\infty)$ is the buoyancy ratio, $Pr = \nu/\alpha$ is the Prandtl number, $Sc = \nu/D$ is the Schmidt number, $D_f = DK_T(C_0 - C_\infty)/C_SC_P\nu(T_0 - T_\infty)$ is the Dufour number, and $S_r = DK_T(T_0 - T_\infty)/\nu T_m(C_0 - C_\infty)$ is the Soret number.

A close look at Eq. (11) reveals that, in mixed convection due to viscous fluid, the velocity profile is not similar because the x-coordinate cannot be eliminated from this equation. Although local non-similarity solutions have been found for some boundary layer flows dealing with viscous fluid, the technique is hard to extend in this case. Thus, for ease of analysis, it was decided to proceed with finding local similarity solutions for the governing equation, Eq. (11). That is, taking $X = x/L$ and then one can still study the effects of various parameters on different profiles at any given X-location.

Boundary conditions (5) in terms of f, θ, and ϕ become

$$\eta = 0:\ f = 0,\ f' = 1,\ \theta = 1,\ \phi = 1 \tag{14a}$$

$$\eta \to \infty:\ f' = 0,\ \theta = 0,\ \phi = 0 \tag{14b}$$

The wall shear stress, heat and mass transfers, respectively, acting on the surface in contact with the ambient fluid of constant density are given by

$$\tau_w = \mu\left(\frac{\partial u}{\partial y}\right)_{y=0},\ q_w(x) = -k\left(\frac{\partial T}{\partial y}\right)_{y=0} \text{ and } q_m(x) = -D\left(\frac{\partial C}{\partial y}\right)_{y=0}$$

where k is the thermal conductivity.

The non-dimensional skin friction $C_f = 2\tau_w/\rho U_*^2$, the local Nusselt number $Nu_x = xq_w(x)/k(T_w(x) - T_\infty)$, and local Sherwood number $Sh_x = xq_m(x)/D(C_w(x) - C_\infty)$ where U_* is the characteristic velocity, are given by

$$C_f\sqrt{\mathrm{Re}_x} = \sqrt{2X}\ f''(0),\ \frac{Nu_x}{\sqrt{\mathrm{Re}_x}} = -\sqrt{\frac{X}{2}}\ \theta'(0) \text{ and } \frac{Sh_x}{\sqrt{\mathrm{Re}_x}} = \sqrt{\frac{X}{2}}\ \phi'(0) \tag{15}$$

where $\mathrm{Re}_x = u_w(x)x/\nu$ is the local Reynolds number based on the surface velocity.

3. Numerical Procedure

The system of non-linear ordinary differential Eqs. (11)–(13) together with the boundary conditions (14) are locally similar and solved numerically using the Keller-box implicit method discussed in Refs. 18 and 19. This method has been proven to be adequate and give accurate results for boundary layer equations. The method has the following four main steps:

Reduce the system of Eqs. (11) to (13) to a first order system;

Write the difference equations using central differences;

Linearize the resulting algebraic equations by Newton's method and write them in matrix-vector form;

Use the block-tridiagonal-elimination technique to solve the linear system.

This method has a second-order accuracy, is unconditionally stable, and is easily programmed, thus making it highly attractive for production use. A uniform grid was adopted, which is concentrated towards the wall. The calculations are repeated until some convergent criterion is satisfied and the calculations are stopped when $\delta f_0'' \le 10^{-8}$, $\delta\theta_0' \le 10^{-8}$, and $\delta\phi_0' \le 10^{-8}$. In the present study, the boundary conditions for η at ∞ are replaced by a sufficiently large value of η where the velocity, temperature, and concentration approach zero. In order to see the effects of step size ($\Delta\eta$) we ran the code for our model with three different step sizes as $\Delta\eta = 0.001$, $\Delta\eta = 0.01$, and $\Delta\eta = 0.05$ and in each case we found very good agreement between them on different profiles. After some trials we imposed a maximal value of η at ∞ of 15 and a grid size of $\Delta\eta$ as 0.01.

4. Results and Discussion

In the present study we have adopted the following default parameter values for the numerical computations: $Pr = 1.0$, $Sc = 0.22$, $\mathrm{Re} = 200$, $\varepsilon = 0.6$, and $B = 0.5$. These values are used throughout the computations, unless otherwise indicated.

In the absence of mixed convection parameter Ri, Forchheimer number Fs, Soret number S_r and Dufour number D_f with $B = 0$, $\varepsilon = 1$, $Da \to \infty$, and $Sc \to 0$ for different values of Prandtl number Pr, the results have been compared with the special case of Magyari and Keller [2] and found to be in good agreement, as shown in Table 1.

Table 1. Comparison between Wall-Temperature Gradient $\theta'(0)$ Calculated by the Present Method and that of Magyari and Keller [2] for $Ri = Fs = S_r = D_f = B = 0$, $Da \to \infty$, $\varepsilon = 1$, and $Sc \to 0$

Pr	*Magyari and Keller [2]*	*Present*
0.5	-0.59434	-0.59438
1.0	-0.95478	-0.95478
3.0	-1.86908	-1.86908
5.0	-2.50014	-2.50015
8.0	-3.24213	-3.24218
10.0	-3.66038	-3.66043

Figure 2 shows the dimensionless velocity profile for various values of the mixed convection parameter *Ri* for fixed values of *Fs*, *Da*, S_r, D_f, and *X*-location. The mixed convection flow governing parameter is positive when the buoyancy is aiding the external flow (aiding flow) and is negative when the buoyancy is opposing the external flow. It reveals that as the value of *Ri* increases, the dimensionless velocity rises. Compared with the limiting case of *Ri* = 0.0 (i.e., pure forced convection), the velocity is more for an aiding flow and the velocity is less for an opposing flow. As *Ri* increases, the buoyancy effects increase and hence the fluid flow accelerates. Figure 3 illustrates the dimensionless temperature for different values of *Ri*. The results indicate that the dimensionless temperature reduces with the increase of *Ri*. The temperature in the case of mixed convection is less for an aiding flow and more for an opposing flow compared to that of pure forced convection. This is due to the fact that when *Ri* (i.e., buoyancy effects) increases, the convection cooling effect increases and hence the temperature reduces. The effect of mixed convection parameter *Ri* on the dimensionless concentration is depicted in Fig. 4. It is clear that the concentration of the fluid decreases with the increase of mixed convection parameter *Ri*.

The dimensionless velocity distribution for different values of Forchheimer number *Fs* with $Da = 0.1$, $Ri = 1.0$, $S_r = 2.0$, $D_f = 0.03$, and $X = 3.0$, is depicted in Fig. 5. Since *Fs* represents the inertial drag, an increase in the Forchheimer number increases the resistance to the flow and so a decrease in

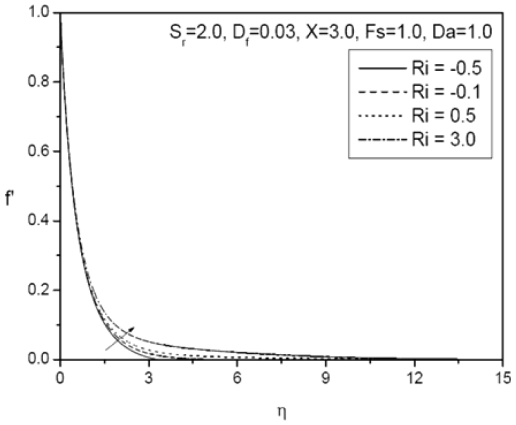

Fig. 2. Velocity profiles for various values of *Ri*.

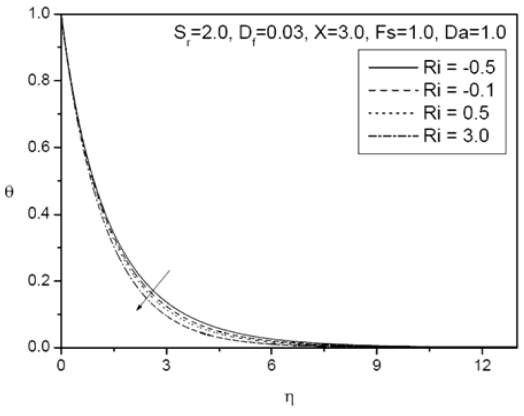

Fig. 3. Temperature profiles for various values of *Ri*.

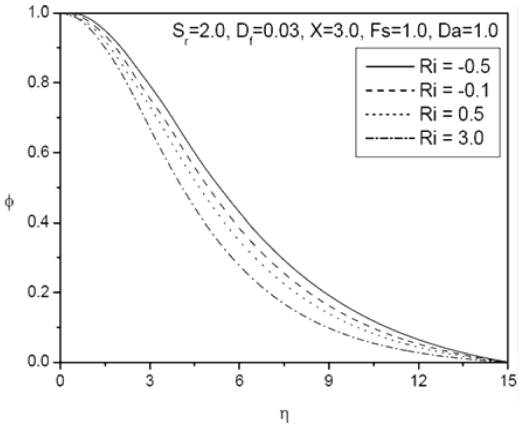

Fig. 4. Concentration profiles for various values of *Ri*.

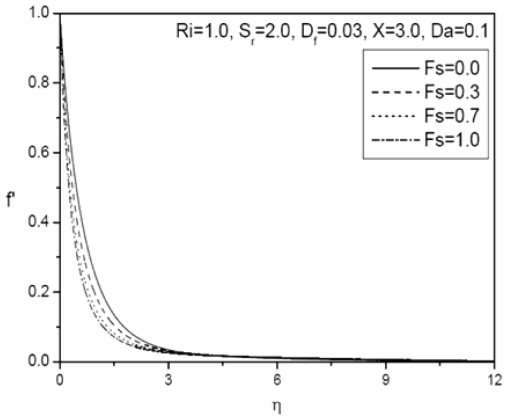

Fig. 5. Velocity profiles for various values of *Fs*.

the fluid velocity ensues. Here $Fs = 0$ represents the case where the flow is Darcian, i.e., inertial effects are neglected and so the velocity is maximum in this case due to the total absence of inertial drag. The dimensionless temperature for different values of the Forchheimer number for fixed values of *Da*, *Ri*, S_r, D_f, and *X*-location, is displayed in Fig. 6. An increase in the Forchheimer number *Fs* increases temperature values, since as the fluid is decelerated, energy is dissipated as heat and serves to increase temperatures. As such the temperature is minimized for the lowest value of *Fs* and maximized for the highest value of *Fs* as shown in Fig. 6. Figure 7 exhibits the dimensionless concentration for different values of the Forchheimer number for fixed values of *Da*, *Ri*, S_r, D_f, and *X*-location. As the Forchheimer number increases, the concentration boundary layer thickness increases. The increase in the non-Darcy parameter reduces the intensity of the flow but enhances the thermal and concentration boundary layer thicknesses.

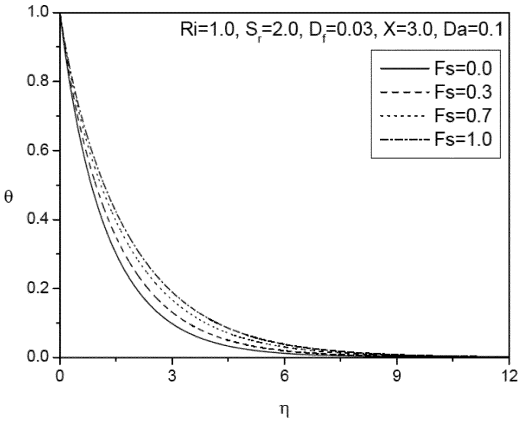

Fig. 6. Temperature profiles for various values of *Fs*.

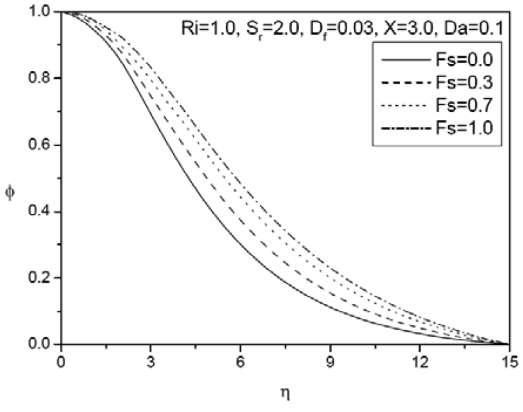

Fig. 7. Concentration profiles for various values of *Fs*.

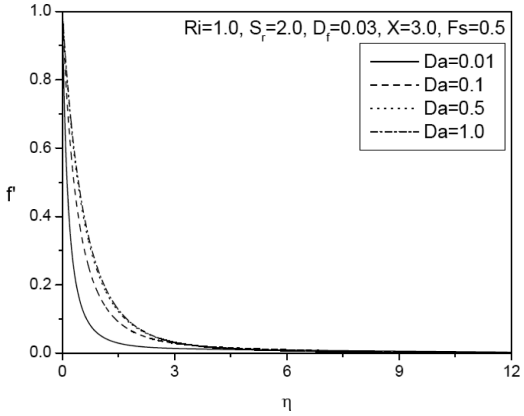

Fig. 8. Velocity profiles for various values of *Da*.

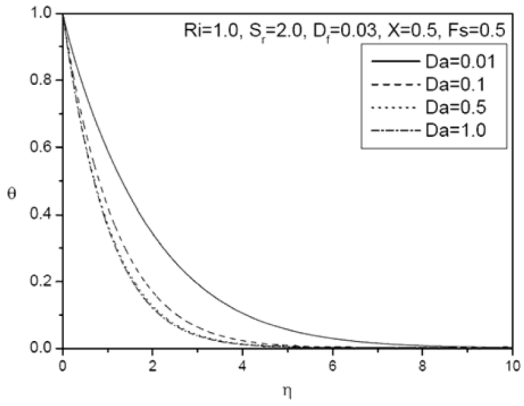

Fig. 9. Temperature profiles for various values of *Da*.

Figures 8 to 10 illustrate the influence of Darcy number *Da* on the velocity, temperature, and concentration profiles. Figure 8 indicates that a rise in *Da* (which implies a rise in permeability, K_p) enhances the velocity of the fluid in the boundary layer. Hence the viscous fluid is increased with a rise in *Da*. With increasing permeability the porous matrix structure becomes less and less prominent and in the limit of infinite *Da* values (i.e., $1/Da \cdot \mathrm{Re} f' \to 0$ and $Fs/Da(f')^2 \to 0$), the porosity vanishes and the present problem reduces to a purely free convective heat and mass transfer in a viscous fluid. Forchheimer drag is clearly inversely proportional to *Da* (and velocity gradient) for constant *Fs*. The dimensionless temperature for different values of Darcy number for $Fs = 0.5$, $Ri = 1.0$, $S_r = 2.0$, $D_f = 0.03$, and $X = 0.5$, is depicted in Fig. 9. It is seen that the temperature of the fluid decreases with the increase in the Darcy number. Figure 10 illustrates the non-dimensional concentration for various values of the Darcy number for $Fs = 0.5$, $Ri = 1.0$, $S_r = 2.0$, $D_f = 0.03$, and $X = 0.5$. It can be seen from the figure that concentration decreases with the increase in the Darcy number.

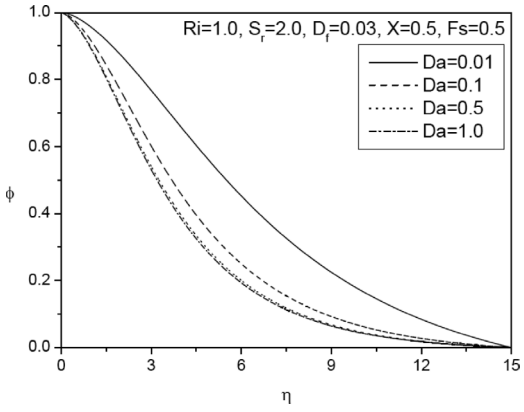

Fig. 10. Concentration profiles for various values of *Da*.

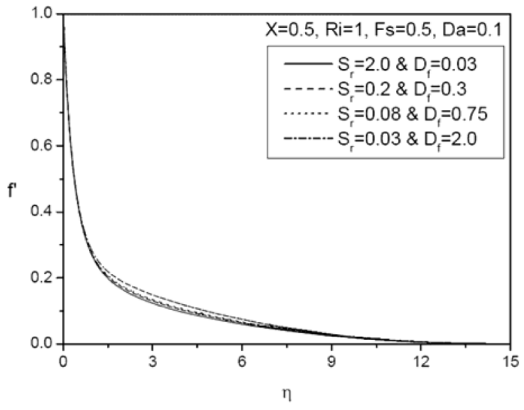

Fig. 11. Velocity profiles for various values of S_r and D_f.

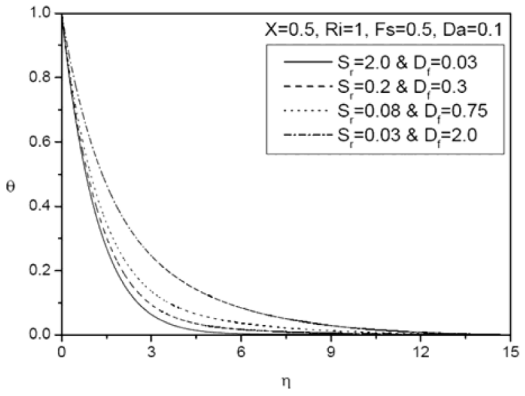

Fig. 12. Temperature profiles for various values of S_r and D_f.

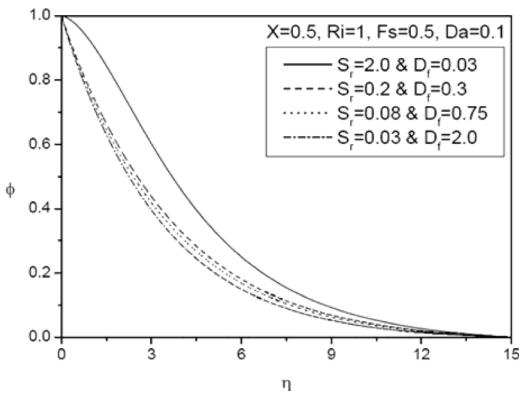

Fig. 13. Concentration profiles for various values of S_r and D_f.

The effects of Soret S_r and Dufour D_f numbers on the velocity, temperature, and concentration profiles in the presence of various physical parameters such as mixed convection, Darcy, and non-Darcy parameters, etc., are depicted in Figs. 11–13. The velocity and temperature profiles increase but the concentration profile decreases with increasing the Soret number S_r (or decreasing with the Dufour number D_f) more effectively near the surface of the stretching sheet, as seen from Figs. 11–13 for fixed values of other parameters. Thus it is concluded from Figs. 11–13 that the velocity, temperature, and concentration distributions are severely affected by the Soret and Dufour effects, especially the thermal boundary layer thickness which increases while the concentration boundary layer thickness decreases with an increase in the Dufour number (or simultaneously decreasing the Soret number). It should be mentioned that the profiles of concentrations are found to be more sensible to the changes with Soret number S_r and Dufour number D_f, respectively. Thus, it is evident that the effects are obviously playing an important role under a mixed convection flow for molecular diffusion through porous medium in the presence of Soret and Dufour effects. Therefore, we understand that the influences of thermal-diffusion as well as the diffusion-thermo effects are extremely effective in the study of mixed convection problems.

In Figs. 14–16, the effects of the X-location on the dimensionless velocity, temperature, and concentration are presented for fixed values of Fs, Da, Ri, S_r, and D_f. From Fig. 14, it is noticed that the velocity decreases with an increase in the value of X-location in the momentum boundary layer. It is clear from Fig. 15 that the thermal boundary layer thickness increases with the increase of X-location but with a significant effect near the stretching sheet. It can be seen from Fig. 16 that the solutal boundary layer thickness of the fluid increases with the increase of X and also found a significant effect within the boundary layer.

The variations of $f''(0)$, $-\theta'(0)$, and $-\phi'(0)$, which are proportional to the local skin-friction coefficient and rate of heat and mass transfers are shown in Table 2 for different values of the physical parameters involved in the problem. The effect of mixed convection parameter Ri with fixed values of Fs, Da, S_r, D_f, and X-location in both cases of opposing and aiding flows are shown in this table. A rapid growth in the non-dimensional skin friction coefficient is noticed with the mixed convection

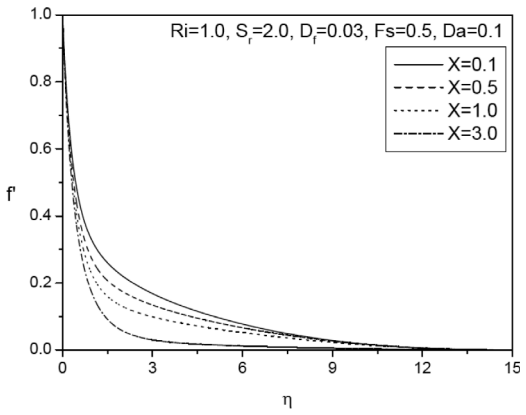

Fig. 14. Velocity profiles for various values of *X*.

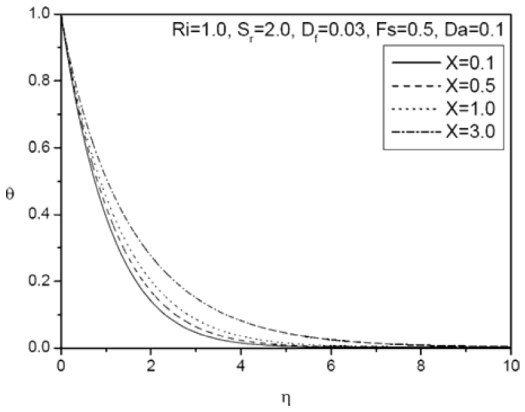

Fig. 15. Temperature profiles for various values of *X*.

parameter *Ri*. The reason is that an increase in the buoyancy effect in a mixed convection flow leads to an acceleration of the fluid flow, which increases the local skin friction factor. Also, it is seen that the heat and mass transfer rates increase in both the cases of opposing and aiding flows with the increasing values of *Ri*. Hence the mixed convection parameter has an important role in controlling the temperature and concentration. The effect of the Forchheimer number *Fs* on the skin friction coefficient $f''(0)$ and heat and mass transfer rates is represented in Table 2. It is observed that the skin friction coefficient and heat and mass transfer rates decrease as *Fs* increases. In Table 2, the effect of the Darcy number *Da*, on the skin friction coefficient $f''(0)$ and heat and mass transfer rates is displayed. It depicts that the skin friction coefficient and heat and mass transfer rates increase as *Da* increases. Table 2 illustrates that, for fixed values of *Fs*, *Da*, S_r, D_f, and *Ri*, the skin friction and heat and mass transfer coefficients are reducing with the increasing values of *X*-location. The values of skin-friction coefficient, local Nusselt number, and local Sherwood number are tabulated in Table 2 for various values of the Soret number and Dufour number. Finally, the effects of the Dufour and Soret number on the local skin-friction coefficient and the rate of heat and mass transfer are shown

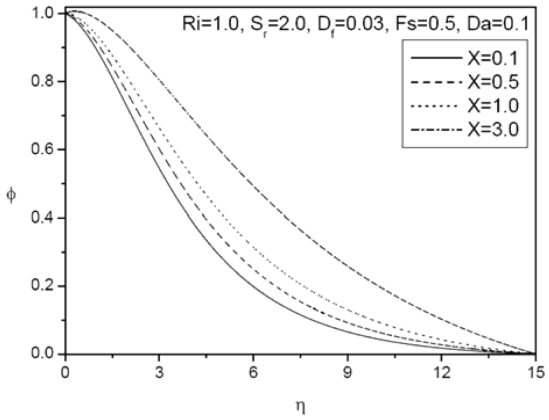

Fig. 16. Concentration profiles for various values of *X*.

Table 2. Effects of Skin Friction, Heat, and Mass Transfer Coefficients for Varying Values of *Ri*, *Fs*, *Da*, S_r, D_f, and *X*

Ri	*Fs*	*Da*	S_r	D_f	*X*	$f''(0)$	$-\theta'(0)$	$-\phi'(0)$
-0.5	1.0	1.0	2.0	0.03	3.0	-1.88352	0.83621	-0.07217
-0.1	1.0	1.0	2.0	0.03	3.0	-1.87820	0.84517	-0.06185
0.5	1.0	1.0	2.0	0.03	3.0	-1.87145	0.85286	-0.05345
3.0	1.0	1.0	2.0	0.03	3.0	-1.84676	0.87161	-0.03528
5.0	1.0	1.0	2.0	0.03	3.0	-1.82852	0.88192	-0.02654
1.0	0.0	0.1	2.0	0.03	3.0	-1.64338	0.88619	-0.04730
1.0	0.3	0.1	2.0	0.03	3.0	-2.25135	0.81091	-0.04960
1.0	0.7	0.1	2.0	0.03	3.0	-2.87295	0.74350	-0.05081
1.0	1.0	0.1	2.0	0.03	3.0	-3.26318	0.70583	-0.05323
1.0	0.5	0.01	2.0	0.03	0.5	-6.44295	0.60236	-0.00084
1.0	0.5	0.1	2.0	0.03	0.5	-2.33645	0.88385	0.015940
1.0	0.5	0.5	2.0	0.03	0.5	-1.54153	0.97319	0.029360
1.0	0.5	1.0	2.0	0.03	0.5	-1.41584	0.98860	0.031920
1.0	0.5	0.1	2.0	0.03	3.0	-2.58060	0.77403	-0.04950
1.0	0.5	0.1	1.6	0.0375	3.0	-2.58068	0.77255	0.009810
1.0	0.5	0.1	1.2	0.05	3.0	-2.58076	0.77033	0.069120
1.0	0.5	0.1	1.0	0.06	3.0	-2.58079	0.76867	0.098780
1.0	0.5	0.1	0.8	0.075	3.0	-2.58083	0.76626	0.128460
1.0	0.5	0.1	0.5	0.12	3.0	-2.58088	0.75933	0.173030
1.0	0.5	0.1	0.2	0.30	3.0	-2.58086	0.73251	0.217900
1.0	0.5	0.1	0.1	0.60	3.0	-2.58076	0.68820	0.233390
1.0	0.5	0.1	2.0	0.03	0.1	-2.15210	0.92793	0.034330
1.0	0.5	0.1	2.0	0.03	0.5	-2.33645	0.88385	0.015940
1.0	0.5	0.1	2.0	0.03	1.0	-2.46268	0.84320	-0.003810
1.0	0.5	0.1	2.0	0.03	3.0	-2.58060	0.77403	-0.049500

in this table. The behavior of these parameters is self-evident from Table 2 and hence is not discussed for brevity.

5. Conclusions

In this paper, a boundary layer analysis for mixed convection heat and mass transfer from an exponentially stretching vertical surface in a viscous fluid-saturated non-Darcy porous medium in the presence of Soret and Dufour effects is analyzed. Using the similarity variables, the governing equations are transformed into a set of set of ordinary differential equations where a numerical solution has been presented for different values of parameters. Compared with the pure forced convection, the velocity is more for the aiding flow and less for the opposing flow in the mixed convection. Also, the temperature and concentration distributions in the case of mixed convection are less for an aiding flow and more for an opposing flow compared to that of pure forced convection. Further, an increase in the mixed convection parameter *Ri*, enhances the skin friction coefficient, non-dimensional heat, and mass transfer coefficients in the boundary layer. An increase in the Forchheimer number *Fs* decreases velocity but increases the temperature and concentration distributions, heat and mass transfer rates, and the local skin friction factor. In the case of Darcy number *Da*, velocity, skin friction, and heat and mass transfer coefficients increase while the temperature and concentration distributions decrease with the increasing values of *Da*. The velocity, temperature profiles, and local mass transfer rate increase in the concentration profile but the local heat transfer rate increases with an increase in the value of the Dufour number (or simultaneous decrease in the Soret number). The skin-friction coefficient increases and then decreases with an increase in the value of the Dufour number (or simultaneous decrease in the Soret number). The velocity and wall temperature distribution are

enhanced but wall concentration distribution, skin friction coefficient, and the rate of heat and mass transfers are reduced with enhancing in the value of the *X*-location in the boundary layer.

Literature Cited

1. Sakiadis BC. Boundary-layer behavior on continuous solid surfaces. AIChE J 1961;7:26–28.
2. Magyari E, Keller B. Heat and mass transfer in the boundary layers on an exponentially stretching continuous surface. J Phys D Appl Phys 1999;32:577–585.
3. Elbahbeshy EMA. Heat transfer over an exponentially stretching continuous surface with suction. Arch Mech 2001;53:643–651.
4. Sajid M, Hayat T. Influence of thermal radiation on the boundary layer flow due to an exponentially stretching sheet. Int Commun Heat Mass Transf 2008;35:347–356.
5. Bidin B, Nazar R. Numerical solution of the boundary layer flow over an exponentially stretching sheet with thermal radiation. European J Sci Res 2009;33:710–717.
6. Nield DA, Bejan A. Convection in porous media, 3rd ed. Springer–Verlag; 2006.
7. Layek GC, Mukhopadhyay S, Samad SkA. Heat and mass transfer analysis for boundary layer stagnation-point flow towards a heated porous stretching sheet with heat absorption/generation and suction/blowing. Int Commun Heat Mass Transf 2007;34:347–356.
8. Hayat T, Abbas Z, Pop I, Asghar S. Effects of radiation and magnetic field on the mixed convection stagnation-point flow over a vertical stretching sheet in a porous medium. Int J Heat Mass Transf 2010;53:466–474.
9. Ali ME, Al-Yousef F. Laminar mixed convection boundary layers induced by a linearly stretching permeable surface. Int J Heat Mass Transf 2002;45:4241–4250.
10. Partha MK, Murthy PVSN, Rajasekhar GP. Effect of viscous dissipation on the mixed convection heat transfer from an exponentially stretching surface. Heat Mass Transf 2005;41:360–366.
11. Pal D. Mixed convection heat transfer in the boundary layers on an exponentially stretching surface with magnetic field. Appl Math Comput 2010;217:2356–2369.
12. Eckert ERG, Drake RM. Analysis of heat and mass transfer. McGraw Hill; 1972.
13. Dursunkaya Z, Worek WM. Diffusion-thermo and thermal diffusion effects in transient and steady natural convection from a vertical surface. Int J Heat Mass Transf 1992;35:2060–2065.
14. Kafoussias NG, Williams NG. Thermal-diffusion and diffusion-thermo effects on mixed free-forced convective and mass transfer boundary layer flow with temperature dependent viscosity. Int J Eng Sci 1995;33:1369–1384.
15. El-Aziz MA. Thermal-diffusion and diffusion-thermo effects on combined heat mass transfer by hydromagnetic three-dimensional free convection over a permeable stretching surface with radiation. Phys Lett A 2008;372:263–272.
16. Ahmed AA. Similarity solution in MHD: Effects of thermal diffusion and diffusion thermo on free convective heat and mass transfer over a stretching surface considering suction or injection. Commun Nonlinear Sci Numer Simul 2009;14:2202–2214.
17. Pal D, Mondal H. Effects of Soret, Dufour, chemical reaction and thermal radiation on MHD non-Darcy unsteady mixed convective heat and mass transfer over a stretching sheet. Commun Nonlinear Sci Numer Simulat 2011;16:1942–1958.
18. Cebeci T, Bradshaw P. Physical and computational aspects of convective heat transfer. Springer-Verlag; 1984.
19. Na TY. Computational methods in engineering boundary value problems. Academic Press; 1979.